Journal of Crystal Growth 598 (2022) 126860

Contents lists available at ScienceDirect

Journal of Crystal Growth

journal homepage: www.elsevier.com/locate/jcrysgro

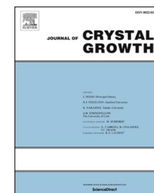

Mid-infrared InAs/InAsSb Type-II superlattices grown on silicon by MOCVD

Richard Brown [a], Bogdan Petrin Ratiu [a], Hui Jia [b], Khalifa M. Azizur-Rahman [c], Manyu Dang [b], Mingchu Tang [b], Baolai Liang [c], Huiyun Liu [b], Qiang Li [a,*]

[a] School of Physics and Astronomy, Cardiff University, Cardiff CF24 3AA, United Kingdom
[b] Department of Electronic and Electrical Engineering, University College London, London WC1E 7JE, United Kingdom
[c] California NanoSystems Institute, University of California, Los Angeles, CA 90095, USA

ARTICLE INFO

Communicated by Hilde Hardtdegen

Keywords:
A3. Metalorganic chemical vapor deposition
B1. Antimonides
B1. Type-II superlattice
B2. III/V on Silicon
A1. Interfacial Misfit Array
B3. Infrared devices

ABSTRACT

In this work we report the growth of the InAs/InAsSb type-II superlattice (T2SL) onto Si substrates via the use of a GaSb/GaAs/Si buffer layer structure all grown by MOCVD. Transmission electron microscopy (TEM) was used to show the effectiveness of the buffer layer structure in reducing threading dislocation density and to verify the formation of an interfacial misfit dislocation array between the GaSb and GaAs layers. Electron channelling contrast imaging was used to measure a threading dislocation density of $6.73 \times 10^8/cm^2$ at the surface of the T2SL. TEM and X-ray diffraction show that the T2SL itself was grown to a high quality considering the large mismatch of the heteroepitaxy. Fourier transform infrared spectroscopy was used to measure the photoluminescence performance of the T2SL which was found to have a FWHM of 50 meV at a peak wavelength of 4.5 μm at 77 K. These results are a step forward towards integration of full InAs/InAsSb T2SL device structures onto Si substrates via MOCVD.

1. Introduction

Infrared devices play an important role in cutting edge applications including gas detection [1], biomedical sensing [2], thermal imaging and 3D sensing [3]. Antimony (Sb) based type-II superlattice (T2SL) materials are a strong candidate for next generation infrared technologies and are now considered as a viable alternative to the state of the art mercury cadmium telluride (MCT) [4]. The Type-II band alignment of the T2SL gives the material system its flexible band gap engineering capability, allowing for widely tuneable wavelength. The T2SL structure is also responsible for the suppression of band-to-band tunnelling, Auger recombination and Shockley-Read-Hall recombination which make up a large proportion of the dark current in MCT [5]. The last big advantage of the T2SL when compared to MCT is in its growth uniformity. The ability to utilise standard III/V growth techniques such as molecular beam epitaxy (MBE) and metal–organic chemical vapor deposition (MOCVD) to grow material with good uniformity is a big advantage for the T2SL when compared to MCT.

There are two main candidates for the Sb based T2SL, the InAs/GaSb T2SL and the InAs/InAsSb T2SL. Historically the focus has been around the InAs/GaSb T2SL due to its larger optical absorption and larger wavelength range [6]. However, more recently the Ga-free InAs/InAsSb T2SL has emerged as a promising new candidate due to its longer minority carrier lifetime [7] and higher defect tolerance [8], particularly in the mid-wave infrared region.

To date, MBE has been the prevailing technique for growing Sb-containing structures [9–11]. However, the commercial exploitation potential using MOCVD is highly attractive if material and device performance can be improved to close the gap with MBE results [12]. Conventionally, MOCVD growth of InAs/GaSb T2SLs is largely hindered by the volatility of antimonides used for strain balancing at the typical growth temperatures [13]. This challenge is circumvented in Ga-free structures as they do not require extra interfacial strain balancing layers. High quality InAs/InAsSb T2SLs can now be grown on GaSb substrates with increasingly comparable dark current densities and detectivities to those grown via MBE [12,14].

Early studies of InAs/InAsSb T2SL indicate a higher level of defect tolerance compared to bulk materials due to the defect energy levels existing above the conduction band [8]. This makes InAs/InAsSb T2SL a promising candidate for integration on silicon (Si). Si substrates are considerably larger, cheaper and less brittle than GaSb substrates which provides clear economic benefits if the challenges associated with the large 12% lattice mismatch can be overcome. Additionally, unlike GaSb, Si is transparent in the Mid-IR [15]. Direct growth of T2SL on Si may

* Corresponding author.
E-mail address: LiQ44@cardiff.ac.uk (Q. Li).

https://doi.org/10.1016/j.jcrysgro.2022.126860
Received 28 July 2022; Received in revised form 3 September 2022; Accepted 6 September 2022
Available online 20 September 2022
0022-0248/© 2022 The Authors. Published by Elsevier B.V. This is an open access article under the CC BY license (http://creativecommons.org/licenses/by/4.0/).

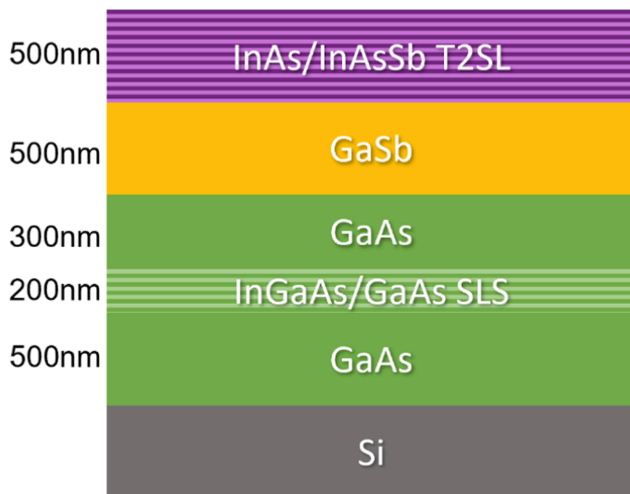

Fig. 1. Schematic diagram of the InAs/InAsSb type-II superlattice grown on (001) Si substrate using the GaSb/GaAs/Si buffer layer structure.

provide a major advantage in the manufacturing of focal plane array detectors which are normally backside illuminated and therefore require a substrate removal step due to the absorption from the GaSb substrate [16]. Recent MBE growth of InAs/InAsSb T2SLs on Si substrates has been demonstrated via the use of AlSb islands at the Si-GaSb interface [17]. However, it is very difficult to grow AlSb via standard MOCVD techniques and up until now, MOCVD growth of defect-tolerant InAs/InAsSb T2SLs on silicon has not been demonstrated. In this paper we report MOCVD growth of Mid-IR InAs/InAsSb T2SLs on Si substrates via the use of a GaSb/GaAs/Si buffer layer structure as shown in Fig. 1. This growth is the first step towards the integration of T2SL based mid-IR detectors on Si substrates grown entirely by MOCVD, which would provide a cost-effective manufacturing route for mid-IR detectors. The T2SL that was grown on Si showed good photoluminescence (PL) characteristics similar to MBE equivalents grown on GaSb [18,19], with a FWHM of 50 meV at a peak wavelength of 4.5 μm at 77 K. The buffer layer structure was shown to be effective in reducing threading dislocation density (TDD), resulting in a TDD of $6.7 \times 10^8/\text{cm}^2$ at the surface of the T2SL.

2. Experiments

The MOCVD growth was performed in an Aixtron Closed Couple Showerhead MOCVD Reactor. The precursors used were triethylgallium (TEGa), tertiarybutylarsine (TBAs), trimethylindium (TMIn) and triethylantimony (TESb) with hydrogen used as the carrier gas. The reactor pressure was 100 mbar. The (001) Si substrates used had a 0.8° offcut and were annealed at 815 °C for 15 min prior to GaAs nucleation to promote a diatomic-stepped surface to prevent antiphase domain formation caused by the polar/non-polar interface [20,21]. After the annealing, GaAs was grown using a two-step growth method comprising of a low temperature nucleation layer at 375 °C and a higher temperature growth at 550 °C. The V/III ratio of the GaAs was 21. A 10 period $In_{0.1}Ga_{0.9}As/GaAs$ strained layer superlattice (SLS) was grown in the GaAs layer to act as a dislocation filtering layer (DFL). This was followed by the growth of GaSb onto the GaAs, where an interfacial misfit dislocation array (IMF) was formed, helping overcome the 7.8% lattice mismatch between GaAs and GaSb. To promote the formation of the 90° dislocations and to minimise the formation of the 60° dislocations [22], starting with a flat and Ga-rich surface of GaAs is critical. This was done by adding an As-desorption step where the TBAs was switched off and the sample was held at 520 °C for 40 s [20,23]. After that, an Sb soaking step was used where the TESb precursor was introduced into the reactor for 30 s to form a monolayer of GaSb. Then the TEGa flow was reopened and 500 nm of GaSb was grown. The V/III ratio of the GaSb was 1.5. The IMF was inspected via high-resolution transmission electron microscopy (TEM) which will be discussed shortly. Once the buffer layer was grown, the final step was to grow the InAs/InAsSb T2SL. This was done at 460 °C by modulating TESb gas flow whilst keeping TBAs and TMIn flowing. TESb flow was switched on for 10 s and then turned off for 23 s, which was repeated 50 times to create a 50 period T2SL. The V/III ratio was 10 for InAs and 15 for InAsSb with an TBAs:TESb flow ratio of 0.7:0.3.

3. Results and discussion

X-ray diffraction (XRD) analysis was performed on the sample to confirm its layer composition and to gain insights into its structure, shown in Fig. 2. From the XRD fitting, the GaSb was found to be 101% relaxed and the GaAs 104% relaxed implying there was a small in-plane tensile strain. This over relaxation was attributed to the mismatch of thermal expansion coefficients. While the sample was cooling down from growth temperature to room temperature, the lattice of GaAs and GaSb shrunk faster than Si, producing this residual tensile stress. The thicknesses of the T2SL layers were found to be 14 ML for the InAs layer and 6 ML for the InAsSb layer. The composition of the grown InAsSb was found to be $InAs_{0.75}Sb_{0.25}$.

Cross-sectional transmission electron microscopy (TEM) was used to examine the buffer layer structure and to investigate the IMF. The TEM results show a clear reduction of TDD from the Si/GaAs interface up to

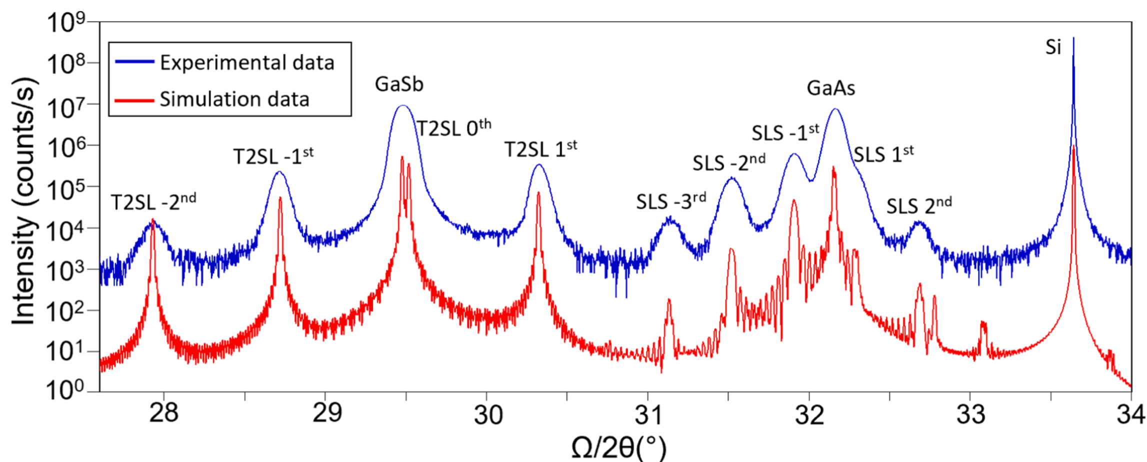

Fig. 2. Experimental and simulated XRD data of the InAs/InAsSb T2SL integrated onto a Si substrate. The thicknesses of the T2SL layers were found to be 14 ML for the InAs layer and 6 ML for the InAsSb layer. The composition of the grown InAsSb was found to be $InAs_{0.75}Sb_{0.25}$.

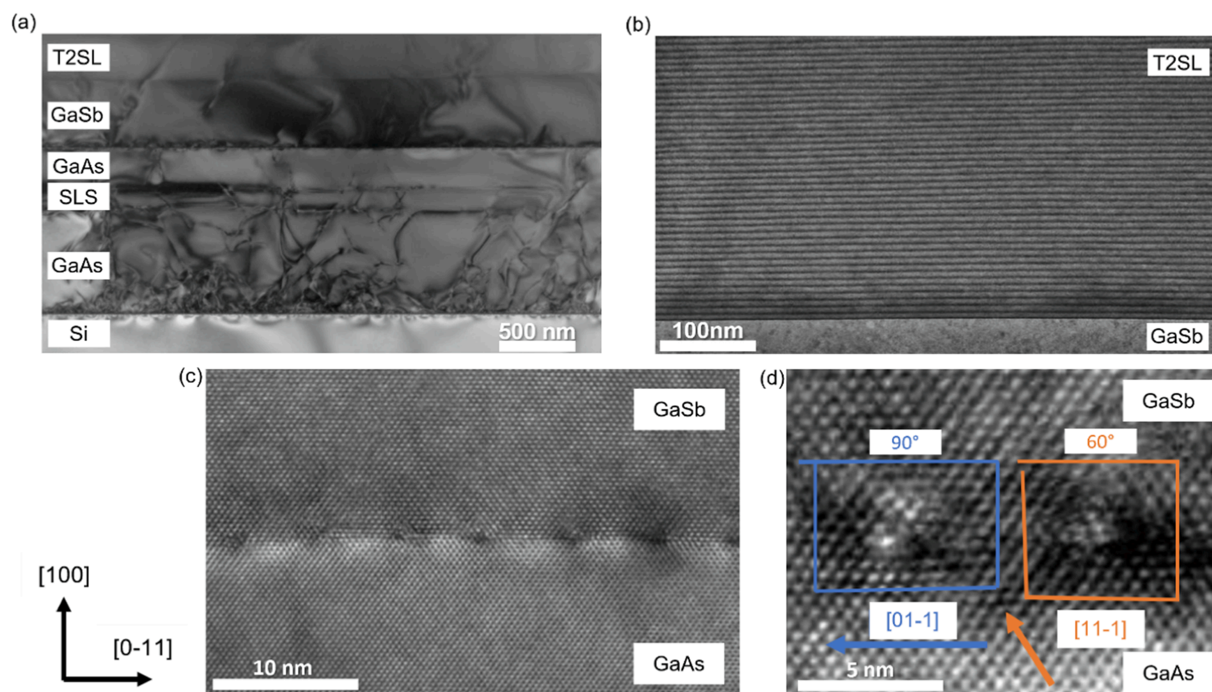

Fig. 3. Cross-sectional TEM image of (a) the whole structure showing a reduction in dislocation density from the GaAs/Si to the T2SL. (b) The T2SL showing distinct stripes indicative of high quality T2SL growth. (c) The GaSb/GaAs interface clearly showing the formation of the IMF. (d) High-resolution TEM image of the misfit dislocations showing both an example of a 90° (blue) and 60° (orange) misfit dislocation and the burgers circuit used to identify them. (For interpretation of the references to colour in this figure legend, the reader is referred to the web version of this article.)

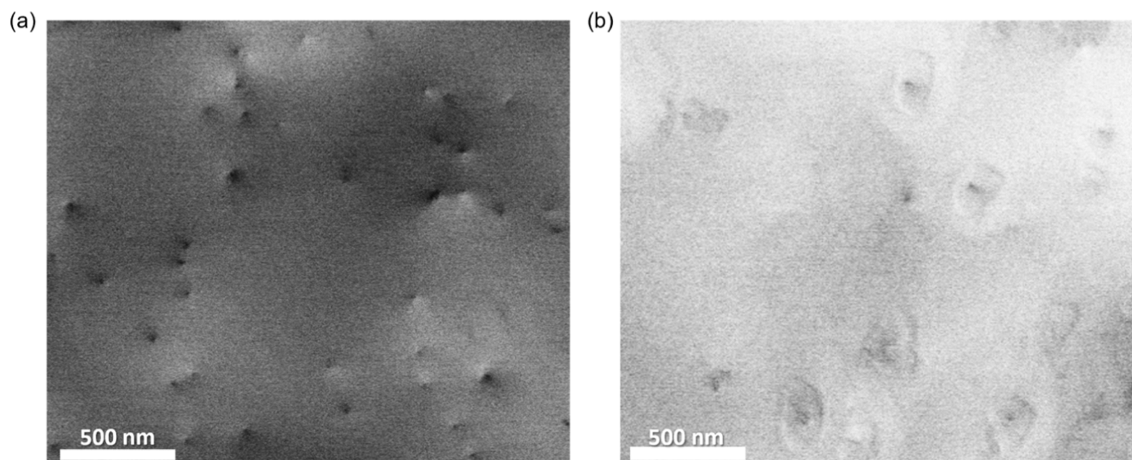

Fig. 4. Electron channelling contrast image of the (a) GaSb surface before T2SL growth with a TDD of $8.4 \times 10^8/cm^2$ and (b) the final T2SL surface with a TDD of $6.7 \times 10^8/cm^2$.

the T2SL as can be seen in Fig. 3a. Fig. 3a also shows clear examples of the SLS bending the threading dislocations parallel to the SLS which prevents them from traveling up into the T2SL. The T2SL itself was then directly investigated via TEM as shown in Fig. 3b, with clear distinct layers observed. The GaSb/GaAs hetero-interface and the formation of the IMF was confirmed in Fig. 3c. The spacing of the misfits was found to be 5.6 nm which indicates one misfit for every 14 GaAs or 13 GaSb lattice sites, in good agreement with previously reported results [22]. Higher resolution TEM was then used to verify the nature of the IMF as can be seen in Fig. 3d. Burgers circuit analysis [24] was performed on 66 different misfit dislocations across the IMF, 34 of which were identified as 90° dislocations and 32 of which 60° dislocations. The same analysis was performed on a sample of GaSb grown directly on GaAs substrate and the IMF of that sample was found to be over 70% 90° dislocations. This difference is attributed to the higher surface roughness and dislocation density of the GaAs on Si in comparison to the native GaAs substrate. Further optimisation of the 2-step GaAs buffer and the $In_{0.1}Ga_{0.9}As$/GaAs DFL could have a knock-on improvement of the GaSb/GaAs interface of our buffer layer structure.

To quantify threading dislocation densities, electron channelling contrast imaging (ECCI) was performed on both the GaSb buffer layer and the complete T2SL structure on Si, as seen in Fig. 4. A total surface area of 120 μm^2 was analysed and an average threading dislocation density of $6.7 \times 10^8/cm^2$ was found at the surface of the T2SL. This TDD is higher than the current state of the art MBE result ($4 \times 10^7/cm^2$), however, further reduction of dislocation density by implementing DFLs within the GaSb layer [17] is possible. The surface roughness was analysed using AFM with scan areas of 5×5 μm^2. The root-mean-square

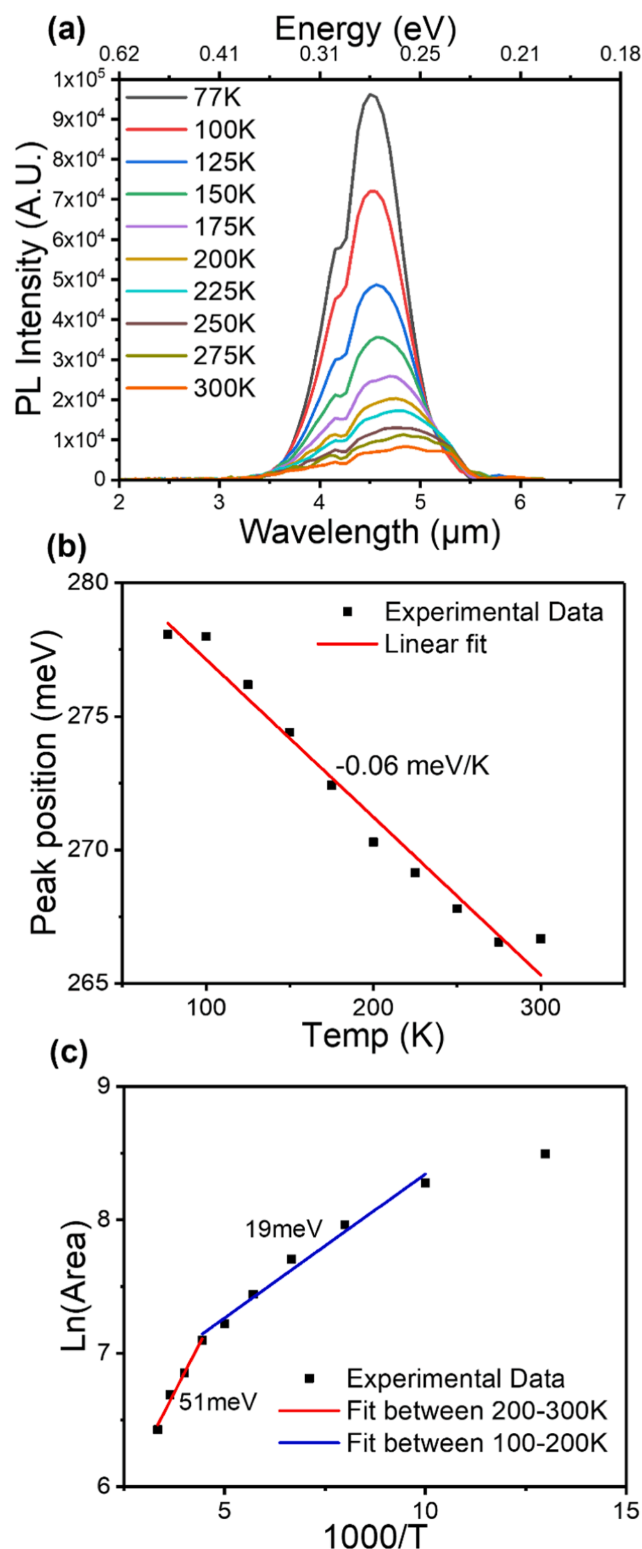

Fig. 5. (a) Temperature dependant PL data of the full T2SL structure. The dip at 4.3 μm is caused by CO_2 absorption in the FTIR. At 77 K the T2SL had a FWHM of 50 meV at a peak wavelength of 4.5 μm (b) Plot showing the temperature dependant redshift of the T2SL (c) Arrhenius plot of the temperature dependant performance used to calculate the activation energy at different temperature ranges.

roughness of the top of the GaSb buffer and the T2SL was found to be 5.8 nm and 7 nm, respectively.

Fourier transform infrared (FTIR) spectroscopy was used to characterise the photoluminescence performance of the T2SL from 77 K to 300 K as shown in Fig. 5a. A 671 nm Diode-Pumped Solid State (DPSS) laser was used to pump the sample to acquire PL. The T2SL exhibited strong PL characteristics with a FWHM of 50 meV at a peak wavelength of 4.5 μm at 77 K. The FWHM was higher than the best values (26 meV) reported from MBE grown T2SL structures on GaSb [25], which is attributed to the higher dislocation density from GaSb buffers on Si. A temperature dependant redshift of −0.06 meV/K was observed which is very similar to previous reports from MBE [18]. An Arrhenius plot was created from the temperature dependant PL data to calculate the activation energy of the non-radiative recombination processes to give an indication of the T2SL quality as shown in Fig. 5c. The fitting was done using the single-channel non-radiative recombination Arrhenius equation:

$$I(T) = \frac{I(0)}{1 + Ce^{-\frac{E_a}{K_B T}}} \tag{1}$$

where $I(0)$ is the integrated PL intensity when the temperature of the T2SL is 0 K, C is a constant, K_B is the Boltzmann constant, T is the temperature, E_a is the activation energy of the non-radiative recombination process. The activation energy was found to be 51 meV between 200 and 300 K and 19 meV between 100 and 200 K. These activation energies are comparable to those grown via MBE on native GaSb substrates [19].

4. Conclusions

The InAs/InAsSb type-II superlattice was integrated onto Si substrates via the use of a GaSb/GaAs/Si buffer layer structure grown entirely via MOCVD. The buffer structure used was shown to be a viable alternative to the current state of the art MBE integration technique. The interfacial misfit dislocation array within the buffer layer was successfully grown with a majority 90° dislocations, leading to a total threading dislocation density of $6.7 \times 10^8/\text{cm}^2$. The InAs/InAsSb T2SL itself was grown to a high quality as shown via TEM. Photoluminescence measurement revealed a FWHM of 50 meV at a peak wavelength of 4.5 μm at 77 K. Although this work is still in its early stages, these initial results may pave the way for the integration of full InAs/InAsSb T2SL device structures onto Si substrates via MOCVD.

CRediT authorship contribution statement

Richard Brown: Writing – original draft, Formal analysis, Investigation, Conceptualization. **Bogdan Petrin Ratiu:** Investigation, Software, Writing – review & editing. **Hui Jia:** Investigation. **Khalifa M. Azizur-Rahman:** Investigation, Writing – review & editing, Formal analysis. **Manyu Dang:** Investigation. **Mingchu Tang:** Investigation. **Baolai Liang:** Investigation, Resources. **Huiyun Liu:** Resources. **Qiang Li:** Supervision, Conceptualization, Resources.

Declaration of Competing Interest

The authors declare that they have no known competing financial interests or personal relationships that could have appeared to influence the work reported in this paper.

Data availability

Information on the data underpinning the results presented here, including how to access them, can be found in the Cardiff University data catalogue at http://doi.org/10.17035/d.2022.0218959420.

Acknowledgements

This work was supported in part by Engineering and Physical Sciences Research Council (grant number EP S024441/1) and in part by the Future Compound Semiconductor Manufacturing Hub (EP P006973/1). Richard Brown acknowledges EPSRC and IQE plc for funding his PhD studentship.

References

[1] D. Popa, F. Udrea, Towards Integrated Mid-Infrared Gas Sensors, Sensors. 19 (2019) 2076, https://doi.org/10.3390/s19092076.
[2] E.F.J. Ring, K. Ammer, Infrared thermal imaging in medicine, Physiol. Meas. 33 (2012) R33–R46, https://doi.org/10.1088/0967-3334/33/3/R33.
[3] S. Nicoletti, J.-M. Fédéli, M. Fournier, P. Labeye, P. Barritault, A. Marchant, A. Glière, A. Teulle, J.-G. Coutard, L. Duraffourg, Miniaturization of mid-IR sensors on Si: challenges and perspectives, in: Silicon Photonics XIV, SPIE (2019) 37–46, https://doi.org/10.1117/12.2506759.
[4] D. Kwan, M. Kesaria, E.A. Anyebe, D. Huffaker, Recent trends in 8–14 µm type-II superlattice infrared detectors, Infrared Phys. Technol. 116 (2021), 103756, https://doi.org/10.1016/j.infrared.2021.103756.
[5] A. Rogalski, HgCdTe infrared detector material: history, status and outlook, Rep. Prog. Phys. 68 (10) (2005) 2267–2336, https://doi.org/10.1088/0034-4885/68/10/R01.
[6] A. Rogalski, P. Martyniuk, M. Kopytko, InAs/GaSb type-II superlattice infrared detectors: Future prospect, Appl. Phys. Rev. 4 (3) (2017) 031304, https://doi.org/10.1063/1.4999077.
[7] E.H. Steenbergen, B.C. Connelly, G.D. Metcalfe, H. Shen, M. Wraback, D. Lubyshev, Y. Qiu, J.M. Fastenau, A.W.K. Liu, S. Elhamri, O.O. Cellek, Y.-H. Zhang, Significantly improved minority carrier lifetime observed in a long-wavelength infrared III-V type-II superlattice comprised of InAs/InAsSb, Appl. Phys. Lett. 99 (2011), 251110, https://doi.org/10.1063/1.3671398.
[8] A.D. Prins, M.K. Lewis, Z.L. Bushell, S.J. Sweeney, S. Liu, Y.-H. Zhang, Evidence for a defect level above the conduction band edge of InAs/InAsSb type-II superlattices for applications in efficient infrared photodetectors, Appl. Phys. Lett. 106 (2015), 171111, https://doi.org/10.1063/1.4919549.
[9] E. Tournié, L. Monge Bartolome, M. Rio Calvo, Z. Loghmari, D.A. Díaz-Thomas, R. Teissier, A.N. Baranov, L. Cerutti, J.-B. Rodriguez, Mid-infrared III–V semiconductor lasers epitaxially grown on Si substrates, Light Sci. Appl. 11 (2022) 165, https://doi.org/10.1038/s41377-022-00850-4.
[10] J.-K. Jiang, Y. Li, F.-R. Chang, S.-N. Cui, W.-Q. Chen, D.-W. Jiang, G.-W. Wang, Y.-Q. Xu, Z.-C. Niu, R. Che, C. Zhang, L. Huang, MBE growth of mid-wavelength infrared photodetectors based on high quality InAs/AlAs/InAsSb superlattice, J. Cryst. Growth. 564 (2021), 126109, https://doi.org/10.1016/j.jcrysgro.2021.126109.
[11] C. González Burguete, D. Guo, P. Jurczak, F. Cui, M. Tang, W. Chen, Z. Deng, Y. Chen, M. Gutiérrez, B. Chen, H. Liu, J. Wu, Direct growth of InAs/GaSb type II superlattice photodiodes on silicon substrates, IET Optoelectron. 12 (2018) 2–4, https://doi.org/10.1049/iet-opt.2017.0078.
[12] D. Wu, Q. Durlin, A. Dehzangi, Y. Zhang, M. Razeghi, High quantum efficiency mid-wavelength infrared type-II InAs/InAs 1–x Sb x superlattice photodiodes grown by metal-organic chemical vapor deposition, Appl. Phys. Lett. 114 (2019), 011104, https://doi.org/10.1063/1.5058714.
[13] X. Li, Y. Zhao, Q. Wu, Y. Teng, X. Hao, Y. Huang, Exploring the optimum growth conditions for InAs/GaSb and GaAs/GaSb superlattices on InAs substrates by metalorganic chemical vapor deposition, J. Cryst. Growth. 502 (2018) 71–75, https://doi.org/10.1016/j.jcrysgro.2018.09.003.
[14] D. Wu, A. Dehzangi, J. Li, M. Razeghi, High performance Zn-diffused planar mid-wavelength infrared type-II InAs/InAs1−xSbx superlattice photodetector by MOCVD, Appl. Phys. Lett. 116 (2020), 161108, https://doi.org/10.1063/5.0005326.
[15] M.M. Milošević, M. Nedeljkovic, T.M. Ben Masaud, E. Jaberansary, H.M.H. Chong, N.G. Emerson, G.T. Reed, G.Z. Mashanovich, Silicon waveguides and devices for the mid-infrared, Appl. Phys. Lett. 101 (2012), 121105, https://doi.org/10.1063/1.4753948.
[16] A. Dehzangi, A. Haddadi, R. Chevallier, Y. Zhang, M. Razeghi, nBn extended short-wavelength infrared focal plane array, Opt. Lett. 43 (2018) 591–594, https://doi.org/10.1364/OL.43.000591.
[17] E. Delli, P.D. Hodgson, M. Bentley, E. Repiso, A.P. Craig, Q. Lu, R. Beanland, A.R. J. Marshall, A. Krier, P.J. Carrington, Mid-infrared type-II InAs/InAsSb quantum wells integrated on silicon, Appl. Phys. Lett. 117 (2020), 131103, https://doi.org/10.1063/5.0022235.
[18] U. Zavala-Moran, M. Bouschet, J.P. Perez, R. Alchaar, S. Bernhardt, I. Ribet-Mohamed, F. de Anda-Salazar, P. Christol, Structural, Optical and Electrical Characterizations of Midwave Infrared Ga-Free Type-II InAs/InAsSb Superlattice Barrier Photodetector, Photonics 7 (2020) 76, https://doi.org/10.3390/photonics7030076.
[19] B.-W. Zhang, D. Fang, X. Fang, H.-B. Zhao, D.-K. Wang, J.-H. Li, X.-H. Wang, D.-B. Wang, InAs/InAsSb type-II superlattice with near room-temperature long-wave emission through interface engineering, Rare Met. 41 (2022) 982–991, https://doi.org/10.1007/s12598-021-01833-x.
[20] Q. Li, K.M. Lau, Epitaxial growth of highly mismatched III-V materials on (001) silicon for electronics and optoelectronics, Prog. Cryst. Growth Charact. Mater. 63 (2017) 105–120, https://doi.org/10.1016/j.pcrysgrow.2017.10.001.
[21] D.J. Chadi, Stabilities of single-layer and bilayer steps on Si(001) surfaces, Phys. Rev. Lett. 59 (1987) 1691–1694, https://doi.org/10.1103/PhysRevLett.59.1691.
[22] A. Jasik, I. Sankowska, A. Wawro, J. Ratajczak, R. Jakieła, D. Pierścińska, D. Smoczyński, K. Czuba, K. Regiński, Comprehensive investigation of the interfacial misfit array formation in GaSb/GaAs material system, Appl. Phys. A. 124 (2018) 512, https://doi.org/10.1007/s00339-018-1931-8.
[23] W. Zhou, W. Tang, K.M. Lau, A strain relief mode at interface of GaSb/GaAs grown by metalorganic chemical vapor deposition, Appl. Phys. Lett. 99 (2011), 221917, https://doi.org/10.1063/1.3663571.
[24] A. Jallipalli, G. Balakrishnan, S.H. Huang, T.J. Rotter, K. Nunna, B.L. Liang, L. R. Dawson, D.L. Huffaker, Structural Analysis of Highly Relaxed GaSb Grown on GaAs Substrates with Periodic Interfacial Array of 90° Misfit Dislocations, Nanoscale Res. Lett. 4 (2009) 1458–1462, https://doi.org/10.1007/s11671-009-9420-9.
[25] J. Kim, H. Yuan, J. Kimchi, J. Lei, E. Rangel, P. Dreiske, A. Ikhlassi, HOT MWIR InAs/InAsSb T2SL discrete photodetector development, Infrared Technol. Appl. XLIV, SPIE (2018) 108–115, https://doi.org/10.1117/12.2303973.